ELSEVIER

Journal of Organometallic Chemistry 565 (1998) 19–28

Journal of Organometallic Chemistry

Preparation and redox properties of phosphite derivatives of $R_2C_2Co_2(CO)_{6-n}[P(OMe)_3]_n$ ($R = CF_3$, MeO_2C)[1]

Noel W. Duffy, C. John McAdam, Brian H. Robinson *, Jim Simpson

Department of Chemistry, University of Otago, P.O. Box 56, Dunedin, New Zealand

Received 5 November 1997

Abstract

A series of phosphite complexes $R_2C_2Co_2(CO)_{6-n}[P(OMe)_3]_n$ ($R = CF_3$, MeO_2C), $n = 1–4$, have been prepared and characterised. Cyclic and square-wave voltammetry shows that the kinetic stability of the radical cations increases with substitution and when $R = CF_3$. The radical cation $\{(CF_3)_2C_2Co_2(CO)_2[P(OMe)_3]_4\}PF_6$ **4a**$^+$ has been characterised and its crystal structure compared with that of the neutral parent. Analysis of the anisotropic ESR spectrum of **4a**$^+$ is consistent with an unpaired electron in a SOMO with little d_z^2 character.

Keywords: Anistropic esr spectrum; Phosphite complexes; Voltammetry

1. Introduction

Reactions of cobalt carbonyl clusters with phosphine and phosphite ligands have led to the formation of a plethora of complexes with a variety of different stoichiometries [1–3] and, in the case of bidentate ligands, coordination geometries. [3–8] A principal feature of these products is the significant effect that substitution can have on the redox properties of the resulting cobalt clusters. Indeed substitution by phosphorus ligands offers the possibility of tuning the cobalt redox centre by controlling the electron density at the metal centre [9], an attractive feature for arrays in which metal carbonyl units feature as the redox centres. In the limit, cluster moieties such as μ-$RCCo_3$ and μ-$R_2C_2Co_2$ can be transformed from readily reducible to oxidisable centres [10–14].

Previous electrochemical studies [12,13] of (μ-R_2C_2)$Co_2(CO)_{6-n}L_n$ clusters concentrated on their cathodic responses. Electrode potential and electrochemical reversibility were found to depend on the order of substitution n and type of ligand L, as well as the acetylene substituent R. The primary electrochemical response is an E_fCE_r mechanism. As the electron withdrawing ability of the capping group increases, the reduction potential decreases, the lifetime of the primary radical anion increases and the redox processes approach chemical reversibility [15]. Unfortunately, the coordination of phosphines and phosphites to the clusters accelerates the decomposition of their radical anions which makes these complexes unsuitable as donor redox centres. In contrast to the reductive electrochemistry, comparatively little is known about the anodic processes of substituted (μ-R_2C_2)$Co_2(CO)_6$ complexes. This paper examines the redox chemistry of the products of sequential phosphite substitution of (μ-R_2C_2)$Co_2(CO)_6$ complexes ($R = CF_3$, MeO_2C), the X-ray structure of $[(CF_3)_2C_2Co_2(CO)_2(P(OMe)_3)_4]^+$ and its neutral parent and ESR spectrum of the radical cation.

* Corresponding author.

[1] Dedicated to Professor Michael Bruce on the occasion of his 60th birthday.

0022-328X/98/$19.00
PII S0022-328X(98)00440-9

2. Results and discussion

2.1. Synthesis of $R_2C_2Co_2(CO)_{6-n}[P(OMe)_3]_n$ ($R = CF_3$, MeO_2C; $n = 1–4$)

Previous work indicated that high yields of monosubstituted derivatives of the alkyne dicobalt complexes could be achieved using electron transfer catalysed substitution reactions [12]. However, thermally-initiated substitution reactions are necessary if the objective is to substitute more than one CO group. New phosphite derivatives of the complex $[\mu\text{-}(MeO_2C)_2C_2]Co_2(CO)_6$, (**1b–4b**) and the highly substituted $[\mu\text{-}(CF_3)_2C_2]Co_2(CO)_6$ derivatives (**1a–4a**) reported earlier [12], were obtained using this strategy (Eq. 1).

$$R_2C_2Co_2(CO)_6 + nP(OMe)_3 \overset{\text{toluene}}{\rightarrow} R_2Co_2(CO)_{6-n}[P(OMe)_3]_n + nCO;\ n = 1–4 \quad (1)$$

The complexes were characterised by elemental analysis and mass spectroscopy (compound numbering follows the value of n in Eq. 1). Infrared spectra of compounds **1–4** show the characteristic fall in the energy of the A_1 ν(CO) band as the carbonyl ligands are replaced by the poorer π-acceptor phosphite ligands with a concomitant build up of electron density in the C_2Co_2 unit. The similarity in the infrared spectra of **1a,b** and **2a,b** with those of other $Co_2(CO)_6$ derivatives suggest that initial substitution of the phosphite ligands occurs at axial sites on each of the two cobalt atoms [3,16]. The preference for axial substitution of monodentate ligands in such compounds has been confirmed by structural [17–19] investigations. Complexes **2a, b** show the 'apparent triplet' in their ^{1}H-NMR, typical of an $X_9AA'X'_9$ spin system seen with di-axial ligand substitution [17,20]. The crystal structure of **4a**, vide infra, shows the presence of two axially and two equatorially substituted phosphite ligands which confirms that the preference for initial axial substitution extends to the more highly substituted derivatives. This contrasts with $Me_2C_2Co_2(CO)_2(dppm)_2$ [14] in which the chelating phosphines are constrained to occupy the four equatorial sites. The ^{31}P-NMR spectrum of **3b** at 223 K had a well-resolved triplet and doublet structure (intensity 1:2, $J = 100–110$ Hz). This fine-structure was unresolved in **3a** which may be due to scrambling between axial and equatorial sites. A single broad ^{31}P resonance in **4a,b**, while confirming the equivalence of the two cobalt coordination spheres, may also arise from ligand scrambling.

2.2. Electrochemistry of *1–4*

Electrochemical data for $R_2C_2Co_2(CO)_{6-n}[P(OMe)_3]_n$ are given in Table 1. When the potential range is extended beyond that incorporating the principle electrode process, additional anodic waves often appear. These show scan rate dependence and $v^{1/2}$ vs. I_p plots typical of phosphite-containing species adsorbed on the electrode surface; these are not discussed herein.

Table 1
Principal electrode processes **A–D** for $R_2C_2Co_2(CO)_{4-n}[P(OMe)_3]_n$[a]

R	n(conc.)/A	B	C	D
CF_3	**1a** (2.2 mM)	**2a** (2.2 mM)	**3a** (3.04 mM)	**4a** (2.4 mM)
E_{pa}/V	1.61	1.22	0.84	0.38
E_{pc}/V	–	1.07	0.75	0.30
MeO_2C	**1b** (1.91 mM)	**2b** (1.85 mM)	**3b** (1.0 mM)	**4b** (1.21 mM)
E_{pa}/V	1.31	1.02	0.64	0.24
E_{pc}/V	–	–	0.54	0.15

[a] Potentials at 20°C vs. SCE (Fc = 0.47 V) in 0.1 M TEAP/acetone). The letters **A–D** correspond to those in Figs. 1–5 in text.

$n = 1$: Cyclic (Fig. 1) and square wave voltammograms of **1a, 1b** are characterised by an irreversible oxidation **A** on both Pt and GC electrodes and over a wide range of scan rate and temperature. Additional waves are seen on anodic and cathodic sweeps due to electroactive fragmentation products (e.g. $Co(CO)_4^-$).

$n = 2$: **2b** gave a similar response to **1b** (Fig. 2), with an irreversible oxidation wave **B** on the anodic sweep but on the cathodic scan wave **C′** was observed, and the corresponding anodic component **C** on subsequent anodic scans. In contrast, I_p^c/I_p^a for **B** in **2a** increases with increasing scan rates (0.17 at 50 mV s^{-1}, 0.60 at 2 V s^{-1}) (Fig. 3), and a non-linear plot of $v^{1/2}$ vs. I_p is consistent with a pseudo-reversible couple.

$n = 3,4$: A pseudo-reversible one-electron oxidation process **C** is observed for **3b** (Fig. 4), $I_p^a/I_p^c = 0.8$ at 200 mV s^{-1} but it approaches unity as the scan rate is increased and a small reversible feature due to couple **D** is observed on cathodic scans. However, the one-electron oxidation process **C** for **3a** is chemically reversible

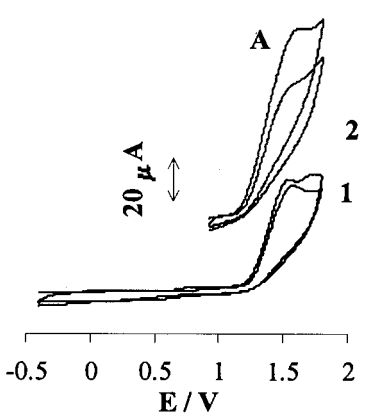

Fig. 1. Cyclic voltammogram of **1a** on Pt at (1) 400 mV s^{-1}, (2) 1000 mV s^{-1}. CH_2Cl_2; 20°C.

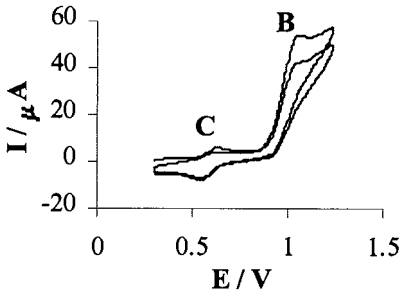

Fig. 2. Cyclic voltammogram of **2b** on Pt, 5 V s^{-1}, CH_2Cl_2, 20°C.

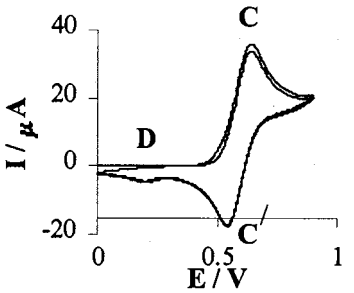

Fig. 4. Cyclic voltammogram of **3b** on Pt at 200 mV s^{-1}, CH_2Cl_2.

with linear plots of $v^{1/2}$ vs. I_p (Fig. 5). The increasing stability of the radical cations with increased substitution culminates at **4a** and **4b** which have electrochemically and chemically reversible one-electron couples **D.** Additional one-electron waves are found for **3a** and **4a, b** ca. 0.6V positive of **C** or **D,** ascribed to oxidation of $\mathbf{3}^+$ and $\mathbf{4}^+$**,** respectively**.** The **3a[2+/+]** couple is chemically irreversible but the **4a,b[2+/+]** couples are partially reversible (I_a/I_c ca. 0.2).

What emerges from these results is that the anodic electrochemical responses are determined by R and the degree of substitution. Potentials for the primary one-electron oxidation step are given by the relationships—$E_{1/2}(V) = 2.02 - n[0.41]$ R = CF_3 and $E_{1/2}(V) = 1.63 - n[0.32]$ for R = $MeCO_2$. For $n = 1 - 3$ formation of the radical cation is followed by chemical and/or EC reactions but the kinetic stability of the cation increases with the degree of substitution, n. For a given n, the μ-$(CF_3)_2C_2$-cluster radical cations have greater stability. The electrochemical profiles for **1–4** at varying scan rates and temperatures are determined by the relative rates of the reactions shown in Scheme 1. The first reaction at the electrode double layer, dominant in **1,** is a fragmentation process resulting in cleavage of the Co–Co bond and liberation of ligand. This reaction is also responsible for the instability of all radical cations $1^+ - 4^+$ in solution at r.t. (vide infra). For complexes **2**,**3** E_fCE_r reactions utilise the liberated ligand from the fragmentation step to generate the $n+1$ complex after the initial scans. In the presence of excess ligand the efficiencies of the E_fCE conversions $2 \rightarrow 3$, $3 \rightarrow 4$ are good and the current ratios are C > > B, D > > C after the initial scans for 2 and 3, respectively. Nevertheless, the phosphite ligand in 4^+ is labile and in the absence of free ligand the reverse conversion $4 \rightarrow 3$ is seen on repeat scans in the cyclic voltammograms for 4. Consequently, complexes **3** and **4** give similar profiles, albeit with different current ratios, with

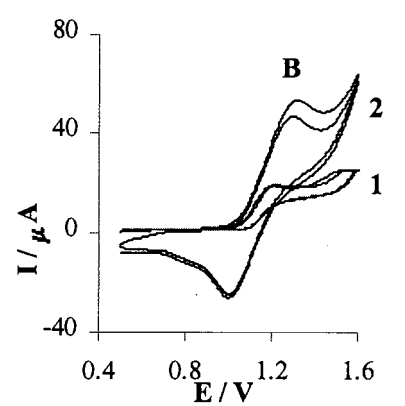

Fig. 3. Cyclic voltammogram of **2a** on Pt, CH_2Cl_2: (1) 400 mV s^{-1} (2) 1000 mV s^{-1}.

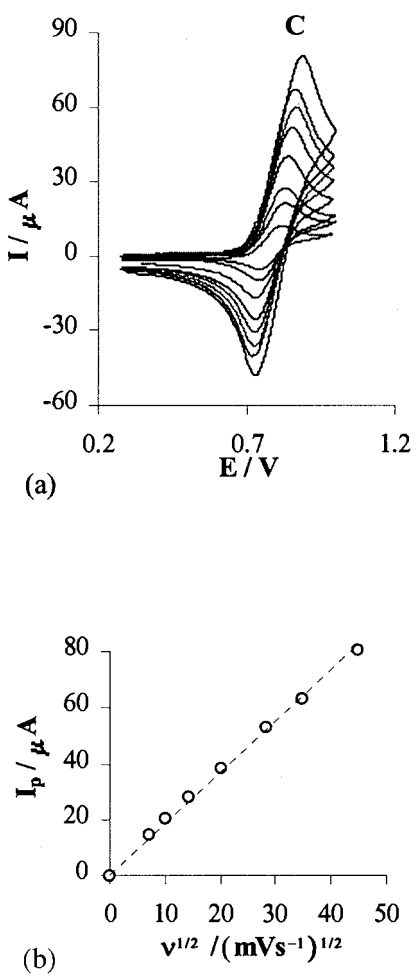

Fig. 5. Cyclic voltammogram of **3a** on Pt at various scan rates from 50–2000 mV s^{-1} (b) Plot of $v^{1/2}$ vs. Ip

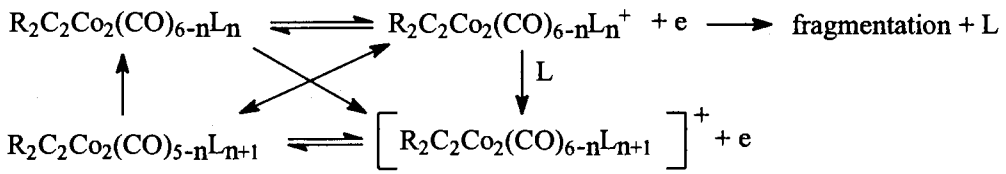

Scheme 1.

both couples C and D incorporated in the cyclic voltammograms.

$$[R_2C_2Co_2(CO)_{6-n}L_n] \overset{e^-}{\rightleftharpoons} [R_2C_2Co_2(CO)_{6-n}L_n]^+$$
$$\overset{k_1}{\rightarrow} \text{fragmentation/loss of L}$$
$$[R_2C_2Co(CO)_{6-n}L_n]^+ + L \overset{k_2}{\rightarrow} [R_2C_2Co(CO)_{6-(n+1)}L_{(n+1)}]^+$$

2.3. Preparation and ESR spectrum of *4a*$^+$

The green cation **4a**$^+$ was prepared by chemical (Ag^+) or electrochemical oxidation and characterised by analysis, mass spectrum and spectroscopy; it was unstable in solution. Equivalent reactions were undertaken with **4b** and **3a** but these products proved even less stable and could not be isolated from solution.

$$(CF_3)_2C_2Co_2(CO)_2[P(OMe)_3]_4 \underset{MeOH}{\overset{Ag^+}{\rightarrow}} \{(CF_3)_2C_2Co_2(CO)_2[P(OMe)_3]_4\}^+ \quad (2)$$

A shift of ca. 40 cm^{-1} in the A_1 ν(CO) band from **4a** to **4a**$^+$ indicates that the electron density on the Co atoms is perturbed by oxidation. This encouraged us to look at the ESR spectrum of **4a**$^+$ as a means of studying the orbital character of the Co–Co bond. Samples of the chemically- or electrochemically-generated cation gave isotropic spectra at ambient temperature. However, the solutions had turned brown at this stage and the isotropic spectra (Fig. 6) were consistent with a monomeric $Co[P(OMe)_3](CO)_x$ species; $g = 2.01469 \pm 0.00002$, with ^{59}Co parameters, $a = 23.498 \pm 0.015$ G and $A = (22.102 \pm 0.015)$ e^{-4} cm^{-1}, and $a = 10.340 \pm 0.071$ G and $A = (9.725 \pm 0.067)e^{-4}$ cm^{-1} for coupling to ^{31}P. A simulation using these values gave a good fit of the experimental spectrum.

A poorly resolved anisotropic spectra (Fig. 7) at 126 K showed little resemblance to the isotropic monomeric spectrum. The anisotropic spectrum is approximately axial with ^{31}P coupling almost equal to the parallel component of the ^{59}Co hyperfine matrix. Least-squares fitting of the resolved parallel components (neglecting the influence of ^{31}P coupling) gave $g_{//} = 2.160 \pm 0.001$, $A_{//} = (55.1 \pm 0.2) \times 10^{-4}$ cm^{-1}. Three perpendicular features attributed to the ^{31}P coupling gave $g_\perp = 2.0464$, $A_P = 49.8 \times 10^{-4}$ cm^{-1}. A simulation with $g_\perp = 2.046$, $g_{//} = 2.160$, $A_\perp^{Co} = 0$, $A_{//}^{Co} = 55$, $A_\perp^P = A_{//}^P = 50 \times 10^{-4}$ cm^{-1} agreed with the experimental spectrum. Assuming that there are no complications arising from non-coincidence of the principal axes of the g- and hyperfine matrices, the relation $A_{//} - \langle A \rangle = P\{\pm 4/7\rho^d + \Delta g_{//} - \Delta\langle g \rangle\}$, where $P = 282 \times 10^{-4}$ cm^{-1}, can be used to calculate ρ^d, the d-electron spin density; the positive sign applies to d_z^2 orbitals, the lower to the other d-orbitals [21]. With $\langle A \rangle = 18.3 \times 10^{-4}$ cm^{-1}, $\Delta\langle g \rangle = 0.082$, ρ^d is 0.095 if $A_{//}$ is positive and 0.361 if $A_{//}$ is negative. The latter results makes more sense as it accounts for 72% of the spin. Thus we conclude that there is not a significant d_z^2 orbital contribution to the

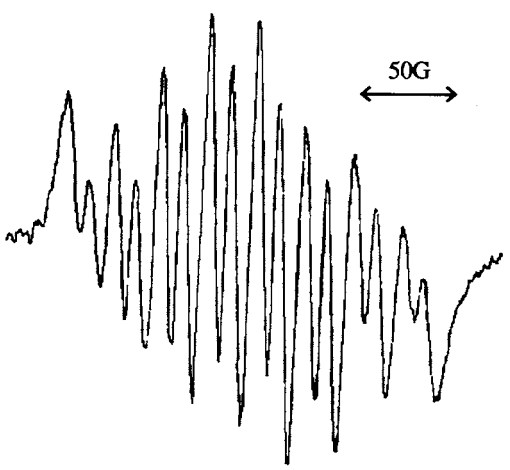

Fig. 6. Isotropic spectrum of product from the electrochemical oxidation of **4a**; 295 K, CH_2Cl_2.

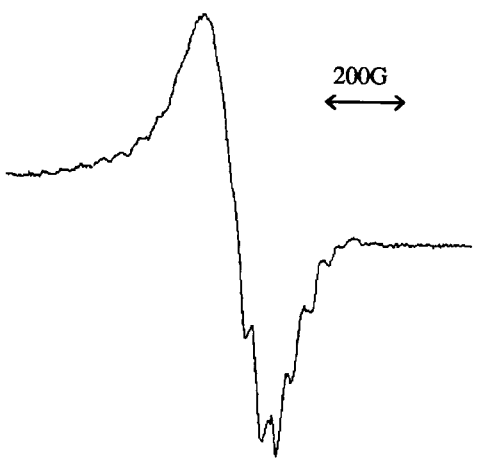

Fig. 7. Anisotropic spectrum of **4a**$^+$ generated by the electrochemical oxidation of **4a;** 126 K, CH_2Cl_2.

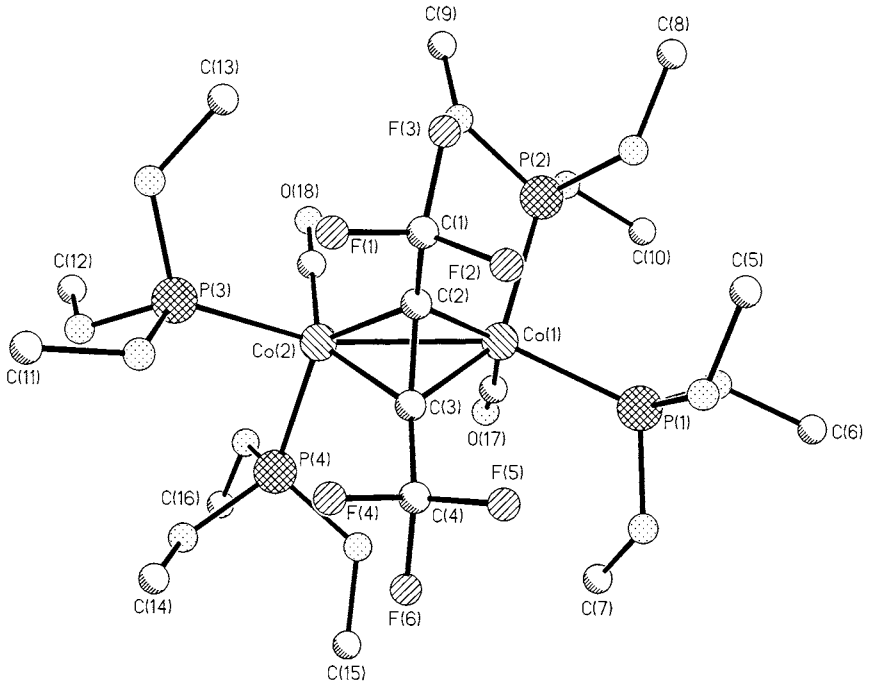

Fig. 8. Perspective view of **4a** showing the atom numbering scheme.

SOMO. This is consistent with the large value of $g_{//}$ which would have been close to g_e with d_z^2 orbital contribution and molecular orbital calculations which suggest that the SOMO is an a_2 orbital essentially antibonding with respect to the cobalt-cobalt bond (vide infra) [22].

2.4. Comparison of the structures of *4a* and *4a*$^+$

An X-ray structural determination of **4a** and **4a**$^+$ provided an opportunity to investigate the structural and electronic effects of one electron oxidation on a (μ-alkyne) complex and to compare these effects with those found in $Me_2C_2Co_2(CO)_2(dppm)_2$ and $\{Me_2C_2Co_2(CO)_2(dppm)_2\}PF_6$ [14].

Perspective views of the neutral and cationic species and the numbering schemes used are shown in Figs. 8 and 9. Selected bond length and angle data are given for **4a** in Table 2 and for **4a**$^+$ in Table 3. The structure of **4a** consists of discrete $(CF_3)_2C_2(CO)_2[P(OMe)_3]_4$ molecules while that of **4a**$^+$ comprises two sets of individual $\{(CF_3)_2C_2(CO)_2[P(OMe)_3]_4\}^+$ cations and PF_6^- anions held together by electrostatic forces. The discrete cations and anions in **4a**$^+$ show minor variations in bond lengths and angles and also in the orientation of the phosphite ligands. Unless otherwise stated, molecular parameters for molecule 1 of **4a**$^+$ will be used in the subsequent discussion.

Complex **4a** has the classic (μ-alkyne)dicobalt unit with the isolobal set of two alkyne carbon atoms and the two Co atoms forming a pseudo-tetrahedral cluster core. In **4a** this core deviates slightly from idealised C_{2v} symmetry with the Co–Co and C–C bonds twisted by 3.1(6)° from the anticipated orthogonal relationship. The distortion is further reflected in the Co–C bond lengths [Co(1)–C(2) 1.918(11); Co(1)–C(3) 1.947(11); Co(2)–C(2) 1.961(10); Co(2)–Co(3) 1.897(12) Å] and the C(1)–C(2)–C(3)–C(4) torsion angle 5(2)°. This may result from steric factors, in particular, the need to minimise repulsion between the CF_3 substituents and the OCH_3 groups of the axially substituted phosphite ligands. Each cobalt atom carries two phosphite ligands, one in an axial and the other in an equatorial site. The two equatorial phosphite ligands are bound *trans* with respect to the Co–Co bond. The placement of these phosphite groups contrasts with that observed for the two bidentate phosphine ligands in $R_2C_2Co_2(CO)_2(dppm)_2$ (R = Me, Ph) [14], where each P atom occupies an equatorial site with the bidentate ligands bridging the Co–Co bond. The binding observed in **4a** endorses the characteristic preference for initial coordination of monodentate ligands to an axial site on the cluster unit. In the precursor $R_2C_2Co_2(CO)_6$ complexes, the carbonyl ligands and the cobalt atoms generate a classic 'sawhorse' structure [23] with the equatorial carbonyl groups on adjacent Co atoms in an eclipsed conformation when viewed down the Co–Co bond. The steric demands of the axial and equatorial phosphite ligands preclude an eclipsed ligand conformation in **4a**, and there is a considerable distortion of the equatorial ligands on the adjacent Co atoms, away from this geometry. The variation in the dihedral angles

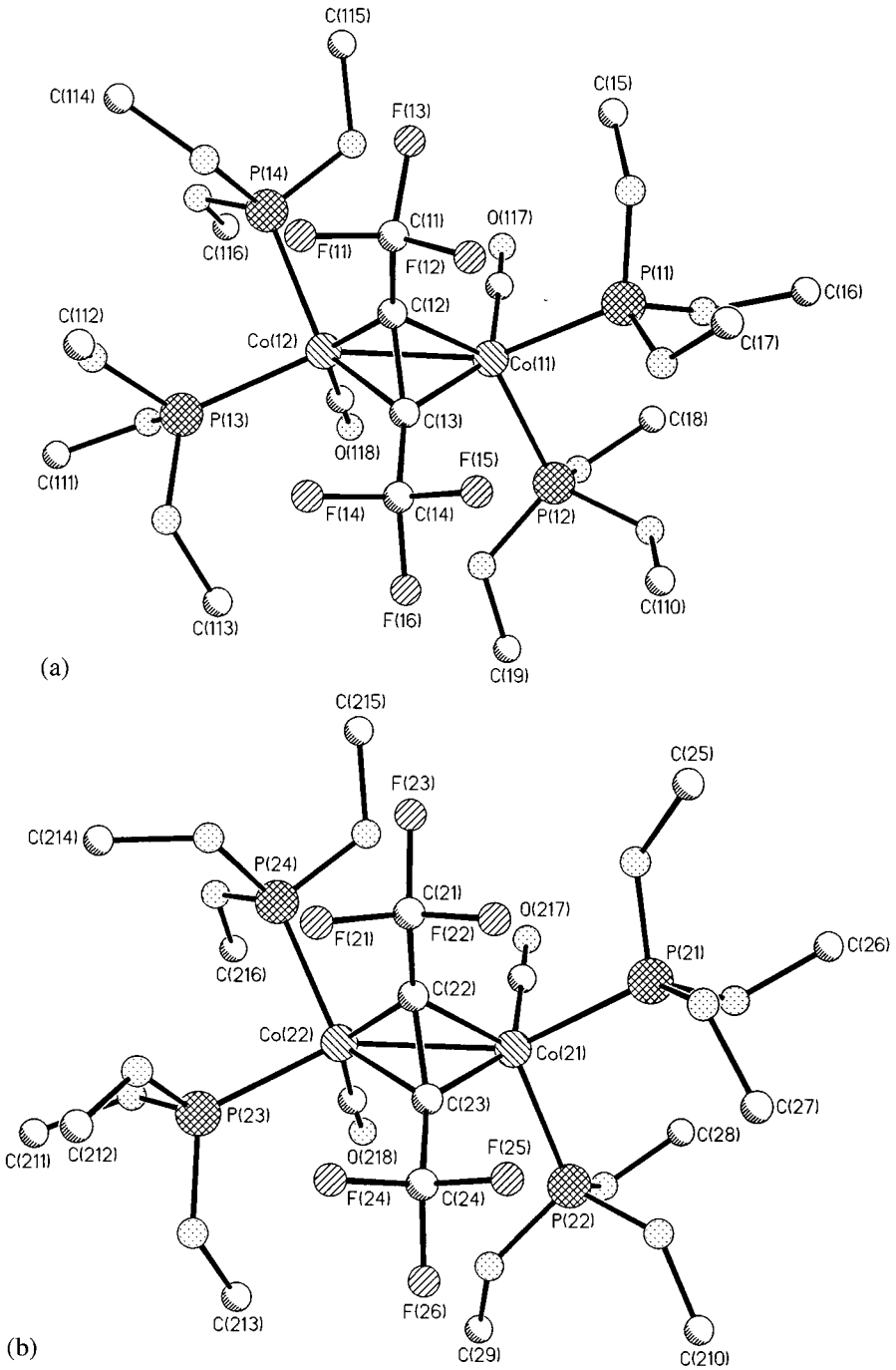

Fig. 9. Perspective views of the two unique cations of **4a**$^+$ showing the atom numbering scheme (a) molecule 1; (b) molecule 2.

C(17)–Co(1)–Co(2)–P(4) 33.2(4) and P(2)–Co(1)–Co(2)–C(18) 37.5(4)° illustrate this. The 'spine' of the saw-horse is also severely distorted with P(1)–Co(1)–Co(2)–P(3) 85.4(3)°.

In the cationic complex, **4a**$^+$, the gross structural features, including the sites of phosphite and carbonyl coordination are unchanged, although considerable distortion of the C_2Co_2 core results from the oxidation process. In **4a**$^+$ the alkyne C–C bond is twisted significantly from the normal transverse relationship to the Co–Co bond with a C(12)–C(13)/Co(11)–Co(12) interline angle of 99.3(3)° [24]. A significant disparity in the Co–C distances in the C_2Co_2 core accompanies this distortion with C(12)–Co(11) 2.036(4), C(13)–Co(12) 2.042(4), C(13)–Co(11) 1.910(4) and C(12)–Co(12) 1.908(4) Å and the C(11)–C(12)–C(13)–C(14) torsion angle increased to 18.1(8)°. This degree of cluster core deformation fits well with the twisting of 12° observed in $\{Me_2C_2Co_2(CO)_2(dppm)_2\}PF_6$ [14]. It is also in accord with the predictions of a rotation of 20–30°

[22,25] for the analogous 32-electron complex $R_2C_2Fe_2(CO)_6$ in which the a_2 orbital of the cobalt complexes (the SOMO for **4a**$^+$) is unoccupied. The structure of *t*-$Bu_2C_2Fe_2(CO)_6$ reveals a much smaller twisting of the alkyne vector relative to the Fe–Fe bond [26], but a major rearrangement of one of the $Fe(CO)_3$ moieties in this molecule effectively reduces the potential for Jahn-Teller distortion by raising the energy of the unoccupied a_2 orbital [22]. It may be significant in this context that the deviation of the equatorial ligands from an eclipsed geometry when viewed down the Co–Co bond increases markedly on oxidation with torsion angles C(117)–Co(11)–Co(12)–P(14) and P(12)–Co(11)–Co(12)–C(118) widened to 45.9(3) and 38.6(1)°, respectively.

Table 2
Selected bond lengths (Å) and angles (°) for **4a** and **4a**$^+$

	4a	**4a**$^+$ Molecule **1**	Molecule **2**
Bond lengths (Å)			
C(1)–C(2)	1.48(2)	1.490(6)	1.474(5)
C(2)–C(3)	1.329(14)	1.345(5)	1.345(5)
C(3)–C(4)	1.49(2)	1.475(5)	1.483(5)
C(2)–Co(1)	1.918(11)	2.036(4)	2.045(4)
C(3)–Co(1)	1.947(11)	1.910(4)	1.900(4)
C(2)–Co(2)	1.961(10)	1.908(4)	1.911(4)
C(3)–Co(2)	1.897(12)	2.042(4)	2.036(4)
Co(1)–Co(2)	2.467(2)	2.3634(9)	2.3652(9)
Co(1)–P(1)	2.148(3)	2.16	78(14)
Co(1)–P(2)	2.163(3)	2.2024(13)	2.1936(14)
Co(1)–C(17)	1.765(13)	1.801(4)	1.795(4)
C(17)–O(17)	1.140(13)	1.135(4)	1.145(4)
Co(2)–P(3)	2.139(4)	2.1763(13)	2.1609(14)
Co(2)–P(4)	2.164(4)	2.1866(13)	2.2033(14)
Co(2)–C(18)	1.756(14)	1.786(4)	1.790(5)
C(18)–O(18)	1.157(13)	1.152(5)	1.147(5)
Bond angles (°)			
C(1)–C(2)–C(3)	134.1(11)	134.1(4)	134.0(4)
C(2)–C(3)–C(4)	130.6(10)	131.2(4)	132.2(4)
C(1)–C(2)–Co(1)	137.2(8)	134.3(3)	137.9(3)
C(1)–C(2)–Co(2)	138.1(8)	142.6(3)	140.6(3)
C(2)–C(3)–Co(1)	68.7(6)	75.2(2)	76.0(2)
C(3)–C(2)–Co(1)	71.1(7)	65.1(2)	64.3(2)
C(2)–C(3)–Co(2)	72.4(7)	64.8(2)	65.1(2)
C(3)–C(2)–Co(2)	67.3(7)	75.6(3)	75.2(2)
C(4)–C(3)–Co(1)	136.7(8)	140.8(3)	140.8(3)
C(4)–C(3)–Co(2)	138.9(8)	139.8(3)	137.9(3)
Co(1)–C(2)–Co(2)	79.0(4)	73.55(13)	73.35(13)
Co(1)–C(3)–Co(2)	79.8(5)	73.35(13)	73.78(13)
P(1)–Co(1)–P(2)	102.66(14)	96.25(5)	100.45(5)
P(1)–Co(1)–Co(2)	148.06(12)	146.53(4)	145.59(4)
P(2)–Co(1)–Co(2)	107.10(11)	115.81(4)	112.63(4)
C(17)–Co(1)–P(1)	96.9(4)	94.88(14)	90.70(13)
C(17)–Co(1)–P(2)	96.3(4)	96.90(13)	99.99(13)
C(17)–Co(1)–Co(2)	91.1(4)	90.76(13)	92.58(13)
Co(1)–C(17)–O(17)	174.6(10)	176.8(4)	178.0(4)
P(3)–Co(2)–P(4)	99.10(14)	92.57(5)	95.55(5)
P(3)–Co(2)–Co(1)	151.52(12)	151.53(4)	146.28(4)
P(4)–Co(2)–Co(1)	106.47(11)	115.36(4)	116.41(5)
C(18)–Co(2)–P(3)	95.7(4)	90.98(13)	95.36(14)
C(18)–Co(2)–P(4)	97.9(4)	105.11(13)	103.58(13)
C(18)–Co(2)–Co(1)	93.1(4)	87.07(12)	87.68(13)
Co(2)–C(18)–O(18)	176.6(11)	179.6(4)	177.5(4)

Table 3
Crystal data and structure refinement for **4a** and **4a**$^+$

	4a	**4a**$^+$
Empirical formula	$C_{18}H_{36}Co_2F_6O_{14}P_4$	$C_{18}H_{36}Co_2F_{12}O_{14}P_5$
Formula weight	832.21	977.18
Temperature (K)	158(2)	130(2)
Wavelength (Å)	0.71073	0.71073
Crystal system	Monoclinic	Monoclinic
Space group	$P2_1/c$	$P2_1/c$
Unit cell dimensions		
a (Å)	17.027(5)	21.203(4)
b (Å)	10.722(2)	16.658(3)
c (Å)	18.220(6)	20.819(4)
β (°)	105.79(3)	96.78(3)
Volume (Å^3)	3201(2)	7302(2)
Z	4	8
D_{calc} (Mg m^{-3})	1.727	1.778
Absorption coefficient (mm^{-1})	1.331	1.246
F(000)	1696	3944
Crystal size (mm)	$0.50\times0.46\times0.18$	$1.2\times0.3\times0.2$
θ range for data collection (°)	2.23–22.52	2.09–22.50
Index ranges	$-18\le h\le3$	$-22\le h\le22$
	$0\le k\le11$	$-17\le k\le0$
	$-19\le l\le19$	$-6\le l\le22$
Reflections collected	5215	15 074
Independent reflections	4196 (R_{int} = 0.1071)	9521 [R_{int} = 0.0173]
Refinement method	Full-matrix least-squares on F^2	Full-matrix least-squares on F^2
Data/restraints/parameters	4193/0/409	9521/0/980
Goodness-of-fit on F^2	1.063	0.928
Final *R* indices [$I>2\sigma(I)$]		
R_1^a	0.0727	0.0356
wR_2	0.1336	0.0806
R indices (all data)		
R_1	0.1474	0.0543
wR_2	0.1698	0.0857
Largest diff. peak and hole (eÅ^{-3})	0.862 and −0.539	0.914 and −0.449

[a] $R_1 = (\Sigma||F_o|-|F_c||/\Sigma|F_o|)$; $wR_2 = [\Sigma w(F_o^2-F_c^2)^2/\Sigma wF_o^4]^{\frac{1}{2}}$.

The C(2)≡C(3) bond in **4a** is 1.329(14) Å long, which is comparable to those observed in various unsubstituted complexes [23] and in the mono and bis-dppm substituted derivatives. On oxidation the corresponding bond in **4a**$^+$ lengthens slightly to 1.345(5) Å. This may reflect the greater involvement of the alkyne π-orbitals in Co–C bonding as a result of the distortion of the C_2Co_2 core. Despite the replacement of four carbonyl ligands with sterically more demanding and poorer π-acceptor phosphite ligands, the Co–Co bond length is 2.467(2) Å in **4a**. This is not appreciably different from those observed in $R_2C_2Co_2(CO)_6$ [R = Ph

2.476(2); MeO_2C 2.477(3); Bu^t 2.460(1) Å] [23] or in alkyne dicobalt complexes with a single dppm ligand bridging the Co–Co bond, where d(Co–Co) is generally in the range 2.46–2.47 Å [27–29]. In sharp contrast, the substitution of a second μ-η^2 dppm ligand results in a significant extension of the Co–Co vector in $R_2C_2Co_2(CO)_2(dppm)_2$ to 2.508(1) Å for R = Ph and 2.513 Å for R = Me [14], perhaps reflecting the increased steric demands of accommodating the bidentate ligands bridging the Co–Co bond. On oxidation, the Co–Co bond length decreases dramatically by more than 0.1 Å, from 2.467(2) Å in **4a** to 2.3634(9) Å in **4a**$^+$. This is in keeping with the Co–Co anti-bonding character of the a_2 HOMO orbital in **4a** from which the electron is removed [22]. Furthermore, the magnitude of the shortening is similar to that observed on oxidation of $Me_2C_2Co_2(CO)_2(dppm)_2$ [14]. Although no other structures of phosphite derivatives of (μ-alkyne)dicobalt complexes have been reported, the Co–P bond distances in **4a** fall within the range observed for phosphite complexes of the isolobally related tricobaltcarbon cluster [30]. The Co–CO bonds are somewhat shorter and the CO bonds longer in **4a** than those reported for the corresponding hexacarbonyl complexes [23]. This reflects the effect of substitution with the poorer π–acceptor phosphite ligands, thus increasing the electron density available in the cluster core for M–CO π-bonding. On oxidation to **4a**$^+$, this electron density is reduced and, as expected, both the Co–P and Co–CO bond distances increase significantly.

2.5. Conclusion

It is clear that an assembly of arrays in which μ-$R_2C_2Co_2$ redox centres are to be used as acceptors will require the coordination of four phosphite ligands per unit if chemical and electrochemical reversibility is to be achieved. Given that two chelating dppm ligands achieve the same effect, but with greater kinetic stability, the only advantage of the phosphite derivatives is the ability to tune into a wide range of potentials.

3. Experimental

$(MeO_2C)_2C_2$ and $AgPF_6$ (Aldrich), $Co_2(CO)_8$ (Merck) and $P(OMe)_3$ (Fluka) were used as received. The complexes μ-$R_2C_2Co_2(CO)_6$, $R = CF_3^+$, MeO_2C^-, were prepared by published procedures [31,32]. Solvents were dried and distilled by standard procedures, and all reactions were performed under oxygen free nitrogen. IR spectra were recorded on a Digilab FX60 spectrometer and NMR on Varian VXR 300 MHz or Gemini 200 MHz spectrometers. ^{1}H-NMR were referenced to $CDCl_3$, and ^{31}P with an external 85% H_3PO_4 standard. Microanalyses were carried out by the Campbell Microanalytical Laboratory, University of Otago. FAB mass spectra were recorded on a Kratos MS80RFA instrument with an Iontech ZN11NF atom gun. Electrospray mass spectra were collected on a VG Platform II mass spectrometer. ESR spectra were recorded on a Bruker ER 220D-LR at Brown University under the guidance of P.H. Rieger and A.N. Rieger. For ESR measurements **4a** in THF:CH_2Cl_2 2:1 (1.5 mmol) was cooled to freezing point in a low temperature ESR cell and **4a**$^+$ generated electrochemically. Electrochemical data was obtained using an EG&G Model 273A potentiostat/galvanostat with a solid Ag/AgCl reference electrode. Solutions were ca. 10^{-3} M electroactive material, 0.10 M $TBAClO_4$ or $TBAPF_6$ supporting electrolyte in CH_2Cl_2, and referenced to the reversible couples [ferrocene]$^{+/0}$ or [decamethyl ferrocene]$^{+/0}$ [33].

3.1. Preparation of *1b–4b*

$MeO_2CC_2CO_2MeCo_2(CO)_6$ (0.23 g, 0.5 mmol) and $P(OMe)_3$ (0.6 g, 5 mmol) were heated under reflux in toluene (50 cm^3) for 1 h. The solvent was removed in vacuo followed by preparative chromatography of the mixture on silica plates (ethyl acetate/hexane (2:1). The products were recrystallised from CH_2Cl_2/hexane. Band 1, $R_f = 0.9$, orange **1b**, 3% yield. Anal. calcd. for $C_{14}H_{15}Co_2O_{12}P$: C, 32.08; H, 2.88; P, 5.91%. Found: C, 32.32; H, 3.04; P, 6.23%. ^{1}H-NMR($CDCl_3$): δ 3.63 (d, $^3J_{P-H} = 12$ Hz, 9H, $-P(OMe)_3$), 3.81 (s, 6H, cluster H). ^{31}P-NMR($CDCl_3$): δ 155 (s). IR(hexane): ν_{CO} 2084 (s), 2043 (vs), 2026 (vs), 1999 (w) cm^{-1}. Band 2, $R_f = 0.6$, orange **2b**, 10% yield. Anal. calcd. for $C_{16}H_{24}Co_2O_{14}P_2$: C, 30.99; H, 3.90; P, 9.99%. Found: C, 30.98; H, 3.89; P, 10.28%. ^{1}H-NMR($CDCl_3$): δ 3.58 (m, $^3J_{P-H} = 12$ Hz, 18H, $-P(OMe)_3$), 3.75 (s, 6H, cluster H). ^{31}P-NMR($CDCl_3$): δ 161 (s). IR(hexane): ν_{CO} 2055 (s), 2016 (s), 1999 (vs), 1986 (w) cm^{-1}. Band 3, $R_f = 0.3$, red **3b**, 55% yield. Anal. calcd. for $C_{18}H_{33}Co_2O_{16}P_3$: C, 30.19; H, 4.64; P, 12.97%. Found: C, 30.25; H, 4.79; P, 13.24%. ^{1}H-NMR($CDCl_3$): δ 3.59 (m, 27H, $-P(OMe)_3$), 3.71 (s, 6H, cluster H). ^{31}P-NMR($CDCl_3$): δ 160 (t, $J = 110$ Hz, 1P), 167 (d, $J = 110$ Hz, 2P). IR(hexane): ν_{CO} 2028 (s), 1987 (vs), 1967 (w) cm^{-1}. Band 4, $R_f = 0.15$, dark red **4b**, 12% yield. Anal. calcd. for $C_{20}H_{42}Co_2O_{18}P_4$: C, 29.57; H, 5.21; P, 15.25%. Found: C, 29.74; H, 5.43; P, 15.02%. *m/e* 812 (M^+), 756 (M^+-2CO), 660 (M^+-CO–$P(OMe)_3$), 632 (M^+-2CO–$P(OMe)_3$). ^{1}H-NMR ($CDCl_3$): δ 3.61 (brs, 36H, $-P(OMe)_3$), 3.67 (s, 6H, cluster H). ^{31}P-NMR ($CDCl_3$): δ 166 (brs). IR (CH_2Cl_2): ν_{CO} 1969 (vs), 1951 (vs) cm^{-1}. Yields of individual derivatives were optimised by varying the ratio of starting cluster to phosphite ligand.

3.2. Preparation of *1a–4a*

A modification of the literature method [12] using excess $P(OMe)_3$ gave improved yields of the higher substituted derivatives (**4a**, 55%). Separation of **1a–4a** was achieved using preparative chromatography on silica with dichloromethane as eluant; products were recrystallised from hexane and identified by microanalysis and from IR spectra in comparison with authentic samples. ^{31}P-NMR ($CDCl_3$): δ 154 [**1a**]; 159 [**2a**]; 164, 159 (2:1) [**3a**]; 164 br. [**4a**].

3.3. Preparation of *4a*$^+$

$AgPF_6$ (80 mg, 0.3 mmol) was added to a solution of **4a** (260 mg, 0.3 mmol) in acetone at r.t. The solution immediately changed from dark red to green and the solvent was removed in vacuo. The residue was rinsed with diethyl ether to remove unreacted cluster, then dissolved in MeOH and filtered through celite. Concentration of this liquor and cooling gave acicular green crystals of **4a**$^+$. Anal. calcd. for $C_{18}H_{36}Co_2F_{12}O_{14}P_5$: C, 22.12; H, 3.71%. Found: C, 22.06; H, 3.54%. Electrospray (m/e): + ve ions, 832 (M^+), 804 (M^+-CO), 776 (M^+-2CO), corresponding peaks [M^+-2CO–$P(OMe)_3$....M^+-2CO–4P$(OMe)_3$]; − ve ion 145 (PF_6^-). IR (KBr): ν_{CO} 2023 (vs), 1988 (s) cm^{-1}.

3.3.1. Electrochemical generation

A solution of 4a (8.0 mM in 0.146 M $TBAPF_6$, $CH_2Cl_2/C_2H_4Cl_2$) was electrolysed just above the freezing point using a two electrode cell with an Au working electrode and a Pt reference electrode. The potential was increased until a current was detected. After 10 min the current had almost ceased and the temperature was lowered to 115 K.

3.4. X-ray data collection, reduction and structure solution for *4a* and *4a*$^+$

Samples of **4a,** recrystallized from CH_2Cl_2/hexane and **4a**$^+$ recrystallised from methanol were prepared as detailed above. A red plate of **4a** and a green block of **4a**$^+$ were used for the data collections. Data were collected on a Siemens diffractometer using graphite moderated Mo–K_α radiation and the w scan technique. Cell dimensions were derived from the angular measurements of 30 strong reflections in the range $3 < 2\theta < 14.5°$. Details of the crystals, data collection and structure refinement are summarized in Table 3. Lorentz polarization and absorption corrections were applied were applied using SHELXTL [34]. Both structures were solved by direct methods using SHELXS-86 [35]; in each case the optimum electron density maps revealed the location of the Co and P atoms together with the majority of the remaining C, O and F atoms. In the case of **4a**$^+$ these included atoms from the two unique molecules in the asymmetric unit. Remaining non-H atoms were located in subsequent difference Fourier, weighted full matrix least-squares refinement cycles using SHELXL-93 [36]. Hydrogen atoms were included as fixed contributions to F_c with fixed isotropic temperature factors. All non-hydrogen atoms were refined anisotropically in both structures. High and increasing temperature factors for four of the F atoms in one of the PF_6^- anions in **4a**$^+$ indicated possible disorder and this was resolved by refining two unique positions for these atoms with their occupancy factors f and f' refined such that $f' = 1 - f$. The final value of f refined to 0.535(16). These structural models converged with $R_1(\Sigma||F_o| - |F_c||/\Sigma|F_o|) = 0.0727$ ($F_1 > 2\sigma F$, 2359 reflections), $wR_2 = [\Sigma w(F_o^2 - F_c^2)^2/\Sigma wF_o^4]^{\frac{1}{2}} = 0.1698$ all data), $S = 1.063$, $w^1 = [\sigma^2(F_o^2) + (0.0459P)^2 + 8.19P$, and $P = (F_o^2 + 2F_c^2)/3$ for **4a** and $R_1 = 0.0356$ ($F > 2\sigma F$, 6982 reflections), $wR_2 = 0.0857$ (all data), $S = 0.928$, $w^1 = [\sigma^2(F_o^2) + (0.0547P)_2$, for **4a**$^+$. The final difference Fourier maps were essentially flat, with maxima at 0.86, − 0.54 eÅ^3 for **4a** and 0.91, − 0.45 eÅ^3 for **4a**$^+$. A full listing of bond lengths and angles, positional and thermal parameters, H atom parameters, observed and calculated structure factors, meanplane data and perspective views of the PF_6^- cations for **4a** and **4a**$^+$. can be obtained from the author (JS).

Acknowledgements

We thank Professor W.T. Robinson, University of Canterbury, for the X-ray data collection, and Dr B.M. Clark, University of Canterbury for the FAB mass spectra and Dr W. Henderson, University of Waikato for the electrospray mass spectra. Special thanks to Professor P.H. and Dr A.N.Rieger for facilitating the ESR measurements and the NSF/NZ Foundation for support to N.W.Duffy.

References

[1] B.R. Penfold, B.H. Robinson, Acc. Chem. Res. 6 (1973) 73.
[2] R.S. Dickson, P.J. Fraser, Adv. Organomet. Chem. 12 (1974) 323.
[3] L.S. Chia, W.R. Cullen, M. Franklin, A.R. Manning, Inorg. Chem. 14 (1975) 2521.
[4] A.J. Downard, B.H. Robinson, J. Simpson, J. Organomet. Chem. 447 (1993) 281.
[5] A.J. Downard, B.H. Robinson, J. Simpson, Organometallics 5 (1986) 1122.
[6] M.J. Don, M.G. Richmond, W.H. Watson, R.P. Kashyap, Acta Crystallogr. Sect. C 47 (1991) 20.
[7] M.J. Don, M.G. Richmond, W.H. Watson, M. Krawiec, R.P. Kashyap, J. Organomet. Chem. 418 (1991) 231.
[8] R.G. Cunninghame, L.R. Hanton, S.D. Jensen, B.H. Robinson, J Simpson, Organometallics 6 (1987) 1470.

[9] B.H. Robinson, J. Simpson, in: M Chanon (Ed.), Paramagnetic Organometallic Species in Activation/Selectivity Catalysis, Kluwer, Dordrecht, Netherlands, 1989, p. 357.
[10] A.M. Bond, P.A. Dawson, B.M. Peake, P.H. Rieger, B.H. Robinson, J. Simpson, Inorg. Chem. 18 (1979) 1413.
[11] S.B. Colbran, B.H. Robinson, J. Simpson, Organometallics 2 (1983) 952.
[12] C.M. Arewgoda, B.H. Robinson, J. Simpson, J. Am. Chem. Soc. 105 (1983) 1893.
[13] C.M. Arewgoda, P.H. Rieger, B.H. Robinson, J. Simpson, S.J. Visco, J. Am. Chem. Soc. 104 (1982) 5633.
[14] (a) R.P. Aggarwal, N.G. Connelly, M.C. Crespo, B.J. Dunne, P.M. Hopkins, A.G. Orpen, J. Chem. Soc. Chem. Commun. (1989) 33. (b) R.P. Aggarwal, N.G. Connelly, M.C. Crespo, B.J. Dunne, P.M. Hopkins, A.G. Orpen, J. Chem. Soc. Dalton Trans. (1992) 655.
[15] C.M. Arewgoda, PhD Thesis, University of Otago, 1981.
[16] G. Varadi, A. Vizi-Orosz, S. Vastag, G. Palyi, J. Organomet. Chem. 108 (1976) 225.
[17] J.-J. Bonnet, R. Mathieu, Inorg. Chem. 17 (1978) 1973.
[18] (a)A. Meyer, A. Gorgues, Y. Le Floc'h, Y. Pineau, J. Guillevic, J.Y. Le Marouille, Tetrahedron Lett., 22 (1981) 5181. (b) D.H. Bradley, M.A. Khan, K.M. Nicholas, Organometallics 11 (1992) 2598.
[19] (a) C.J. McAdam, N.W. Duffy, B.H. Robinson, J. Simpson, J. Organomet. Chem. 527(1997) 179. (b) C.J. McAdam, N.W. Duffy, B.H. Robinson, J. Simpson, manuscript in preparation.
[20] M.J. Church, M.J. Mays, J. Inorg. Nucl. Chem. 33 (1971) 253.
[21] L.G. Casagrande, T.Chen, P.H. Rieger, B.H. Robinson, J. Simpson, S.J. Visco, Inorg. Chem. 23 (1984) 2019.
[22] D. Thorn, R. Hoffmann, Inorg. Chem. 17 (1978) 126.
[23] D. Gregson, J.A.K. Howard, Acta Crystallogr. C39 (1983) 1024.
[24] M. Nardelli, PARST. A system for calculating molecular structure parameters from the results of crystal structure analyses, Comput. Chem. 7 (1983) 95.
[25] A.B. Anderson, Inorg. Chem. 15 (1976) 2598.
[26] F.A. Cotton, J.D. Jamerson, B.R. Stults, J. Am. Chem. Soc. 98 (1976) 1774.
[27] P.H. Bird, A.R. Fraser, D.N. Hall, Inorg. Chem. 16 (1977) 1923.
[28] C.J. McAdam, N.W. Duffy, B.H. Robinson, J. Simpson, Organometallics 15 (1996) 3935.
[29] (a)A. Gelling, J.C. Jeffery, D.C. Povey, M.J. Went, J. Chem. Soc. Chem. Commun. (1991) 349. (b) K.C. Nicolaou, P. Maligres, T. Suzuki, S.V. Wendeborn, W.M. Dai, R.K. Chadha, J. Am. Chem. Soc. 114 (1992) 8890.
[30] P.A. Dawson, B.H. Robinson, J. Simpson, J. Chem. Soc. Dalton Trans. (1979) 1762.
[31] J.L. Boston, D.W.A. Sharp, G. Wilkinson, J. Chem. Soc. (1962) 3488.
[32] U. Krüerke, W. Hübel, Chem. Ber. 94 (1961) 2829.
[33] A.J. Downard, B.H. Robinson, J. Simpson, Organometallics 5 (1986) 1132.
[34] G.M. Sheldrick, SHELXTL: An integrated system for solving, refining and displaying crystal structures from diffraction data., University of Göttingen, Federal Republic of Germany, 1980.
[35] (a) G.M. Sheldrick, SHELXS-86: A program for the solution of crystal structures from diffraction data., University of Göttingen, Federal Republic of Germany, 1986. (b) G.M. Sheldrick, Acta Crystallogr. A46 (1990) 467.
[36] G.M. Sheldrick, SHELXL-93. J. Appl. Cryst. (1993) in preparation.